Impinging Jet Cooling on Concave Surfaces

N. Souris and H. Liakos
Dept. of Process and Systems Analysis Design and Development, CFDU, School of Chemical Engineering, National Technical University of Athens, Zografou, 15780 Athens, Greece

M. Founti
Dept. of Thermal Engineering, Heterogeneous Flows and Combustion Systems, School of Mechanical Engineering, National Technical University of Athens, Zografou, 15780 Athens, Greece

DOI 10.1002/aic.10171
Published online in Wiley InterScience (www.interscience.wiley.com).

The numerical modeling of jet impingement cooling onto a semicircular concave surface is reported. The performance of two-equation turbulence models (such as the k–ε model) is evaluated vs. the Reynolds stress model proposed. The Reynolds-averaged momentum and energy equations are solved together with equations for the turbulence models, using a fully unstructured control volume method and a second-order high-resolution differencing scheme. Variations of jet Reynolds numbers of the spacing between the nozzle and the concave surface, as well as of the distance from the stagnation point in the circumferential direction, are considered. The predicted results are validated against experimental data. The developed approach yields low-cost and accurate predictions of processes where jet impingement cooling is involved. It can assist the design of relevant applications, with relative ease, especially in view of the enhanced heat transfer encountered in the concave surface jet impingement. © 2004 American Institute of Chemical Engineers *AIChE J,* 50: 1672–1683, 2004
Keywords: jet impingement cooling, concave surface, impinging jet, wall jet, k–ε model, Reynolds stress model

Introduction

Impinging jet flows occur in a wide variety of circumstances of practical interest, such as surface coating and cleaning; cooling of electronic components; metal cutting and forming; fire testing of building materials; turbine-blade cooling; and drying of textiles, veneer, paper, and film materials. Numerous studies have been reported on the effects of various parameters (such as the Reynolds number, the nozzle-to-surface distance, the nozzle geometry, the jet temperature and orientation, the number of jets, and the impinging surface shape), on the resulting flow and its heat transfer (Bray, 1992; Garimella and Nenaydykh, 1996; Knowles, 1996; Liu and Sullivan, 1996; Myszko, 1997).

Correspondence concerning this article should be addressed to H. Liakos at hliakos@chemeng.ntua.gr.

Despite the fact that a number of engineering applications, such as turbine blade cooling, deal with impingement on curved surfaces, the majority of previous studies have focused on flat-surface impingement with various configurations of single- or arrays of round and slot nozzles (Jambunathan et al., 1992; Martin, 1977; Viskanta, 1993). In general, works dealing with jets impinging on curved surfaces are limited, compared to the flat-plate investigations, and are mainly focused on experimental heat and/or mass measurements and their theoretical interpretation.

The surface curvature produces the centripetal force by which the flow becomes unstable and a so-called Taylor–Görtler-type vortex is produced (Mayle et al., 1981; Thomann, 1968). This vortex is known to enhance momentum and energy transfer on the surface. Results from the investigations by Thomann (1968) showed that heat transfer on a concave surface is about 20% higher than that on a flat surface. Chup et al. (1969), Metzger et al. (1972), and Tabakoff and Clevenger

(1972) made measurements of impingement cooling on a semicircular surface with an array of round jets and investigated the effects of jet-to-jet spacing, the distance between the jet and the cooled surface, and various jet-hole arrangements. Dyban and Mazur (1970) measured the heat transfer coefficient on a parabolic concave surface and studied the effects of jet-flow passage curvature. Metzger et al. (1972) and Bunker and Metzger (1990) studied heat-transfer characteristics for different leading edge shapes of the cooled surfaces. Hrycak (1981, 1982) reported that the total heat transfer at the stagnation point on the concave surface is higher than that for the flat-surface geometry because of a larger surface area, especially for small nozzle-to-surface distances. Gau and Chung (1991) visualized the jet flow impinging on both convex and concave semicircular surfaces at Reynolds numbers from 6000 to 35,000 and slot width–to-surface diameter ratios of 8–45. Their results indicated that the heat transfer rate on and around the stagnation point increases with increasing relative curvature because of an earlier initiation of vortices in the mixing region of a wider jet, which causes an earlier termination of the potential core and the enhancement in the momentum and energy transport near the wall. In all cases heat transfer is higher than that for an impingement on a flat plate under the same conditions.

Kottke (1997) investigated how disturbances superimposed on the mainstream interacted with the Taylor– Görtler vortex for different mesh type, mesh size, mainstream velocity, and the distance between the mesh and test duct front. Hsueh and Chin (1986) measured mass-transfer rate on a convex cylindrical surface impinged by slot jets.

More recently, Lee et al. (1997, 1999) studied the effects of a hemispherical convex surface curvature on the local heat transfer by a round impinging jet issuing from a long straight pipe nozzle. They found that both the stagnation and the wall-jet region Nusselt number increase with increasing surface curvature. This was attributed to an increased acceleration from the stagnation point for a higher convex surface curvature and to a thinning of the boundary layer caused by the surface curvature and to a generation of Taylor–Görtler vortices, which in turn enhance the heat transfer rate.

Kornblum and Goldstein (1997) examined the flow of circular jets impinging on concave and convex semicylindrical surfaces for small nozzle-to-target surface diameter d/D (0.0197–0.0394). Their flow visualization results, although not detailed enough to show the motion of the ring vortices, indicate a substantial recirculation of the flow exiting the concave surface into the main jet flow. Cornaro et al. (1989) used smoke wire flow visualization to investigate the behavior of a round jet issuing from a straight tube and impinging on concave and convex surfaces with high relative curvature values. Their results confirm those of Kornblum and Goldstein (1997) and indicate the initiation and growth of ring vortices in the jet shear layer and their interaction with the cylindrical surfaces.

Yang et al. (1999) investigated jet impingement cooling on a semicircular concave surface with three different slot nozzles and also studied characteristics of free jets issuing from these nozzles. Their results showed significantly different flow and heat transfer characteristics for the various nozzle shapes tested.

Choi et al. (2000) investigated jet impingement cooling on a semicircular concave surface and presented data for different Reynolds numbers, nozzle-to-surface distances, and distances from the stagnation point in the circumferential direction. The emphasis in their work was placed on the measurement of the turbulent flow characteristics and on interpreting heat transfer data, particularly the occurrence and location of a secondary peak in connection with data of measured mean velocity and velocity fluctuations on the concave surface. Their results showed an increase of the stagnation heat transfer rate for distance from impingement (H) to nozzle slot jet width (B) ratios of 2–3 $< H/B <$ 5–6, which was attributed to the steep increase of velocity fluctuations measured in free and impinging jets.

The prediction of the flow and heat-transfer characteristics in similar cases, using computational fluid dynamics (CFD), can be of considerable practical value and can lead to process optimization. To the best of the authors' knowledge, no numerical predictions have been reported, up to the present, for cases of impinging jets on curved surfaces. The complexities involved in modeling the curved surface and the jet interactions attributed to curvature were the main reasons that hindered accurate numerical simulations in this complex configuration, until recently.

The present study provides numerical predictions for the case of a jet that impinges on a semicircular concave surface with a diameter of 150 mm. The calculations are made for three different Reynolds numbers equal to 1780, 2960, and 4740 and for three different nozzle-to-concave target spacings of H/B values of 4, 6, and 10 (Figure 1), using two different turbulence models: the standard k–ε (Launder and Spalding, 1974) and the Reynolds stress turbulence model of Launder et al. (1975). The parametric variations allow characterization of the flow and validation of the sensitivity of the selected turbulence models in the flow parameters.

The two cited turbulence models are widely used, can offer reliable results, and have general value. They can therefore be applied in this flow where no previous computational experience exists. In general, details of turbulence characteristics can be captured only after careful selection and implementation of an appropriate turbulence model (Liakos et al., 2000a,b). Modified turbulence models (such as modified k–ε models; nonlinear k–ε models; low-Reynolds number models; algebraic models of two, three, or more equations) show their numerical superiority over the standard k–ε, only in specific geometries, and should be implemented on a case-to-case basis. In particular, low-Reynolds number models have been reported to improve predictions in flow fields with streamline curvature (Chien, 1982; Dotoya and Michard, 1981; Hassid and Poreh, 1978; Hoffman, 1975; Lam and Bremhorst, 1981; Launder and Sharma, 1974; Reynolds, 1976; Wilcox and Rubesin, 1980). Their requirement for the first cell to be within the laminar sublayer of the boundary layer still remains their main drawback, which results in increased computational cost. Furthermore, especially because no previous computational work has been carried out on the present subject, a low-Reynolds scheme is not recommended in the current concave geometry, attributed to the nature of the flow, which creates curvature phenomena that affect initial turbulent length estimation needed in low-Reynolds models.

On the other hand, the k–ε model has been used to predict impinging jet flow fields ranging from single impinging jets to three-jet lifting configurations for the next generation of STOVL aircraft (Barata et al., 1989; Bray, 1992; Childs and

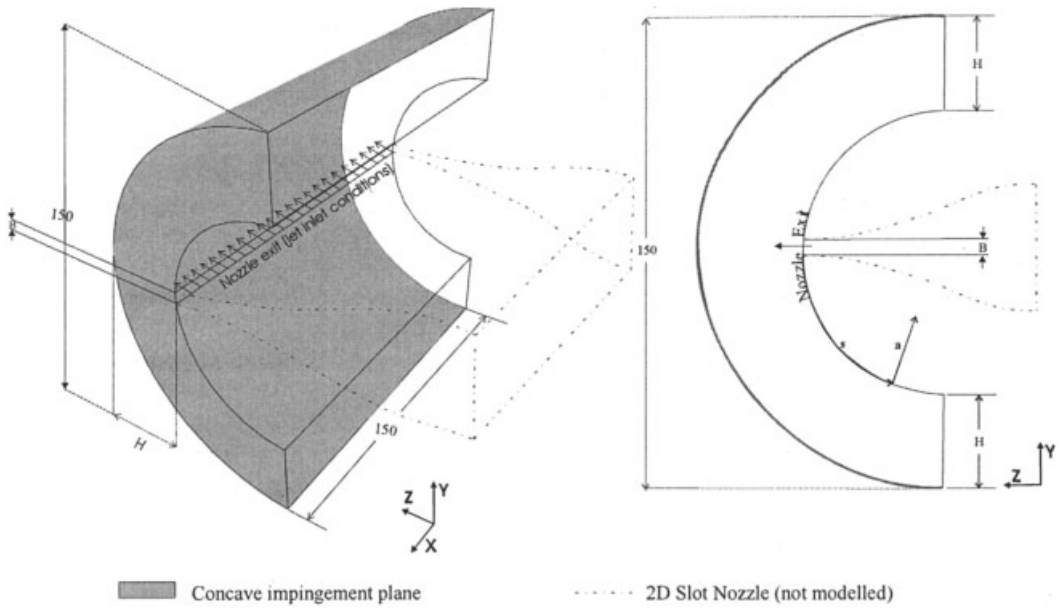

Figure 1. Computational domain.

Nixon, 1987; Craft et al., 1993; Hwang and Liu, 1989; Knowles, 1996). In spite of their wide application, the k–ε-type turbulence models have demonstrated limited accuracy, associated with the nature of the impingement process itself and the use of logarithmic wall functions. To deal with this well-known drawback, Koronaki et al. (2001) tested the nonequilibrium wall functions in geometries with strong curvature. Their results indicated that the use of nonequilibrium wall functions leads to more accurate predictions of the near-wall physical characteristics of the flow.

Based on the preceding remarks, the selection of an appropriate model from among all the available turbulence models for the present case represents a very difficult task. A recent study conducted by the same scientific team (Souris et al., 2002) tested the performance of the low-Reynolds number k–ε model of Launder and Sharma (1974) and of the algebraic stress model (ASM; Rodi, 1976) in flat-plate impingement geometry. Results for the ASM were well validated for impingement effects, whereas the low-Reynolds number model showed its known advantages in the near-wall region. However, because of the lack of previous computational experience on the specific curved geometry, no one can assert with certainty that the flat plate conclusions will also apply to the concave case. Therefore, before making a final selection concerning turbulence modeling, the effect of curvature in relation to that of impingement should be seriously taken into consideration. This actually means that neither a low-Reynolds number nor an ASM can be applied to this concave impingement case without proper calibration of the models in the near-wall region. At the same time, such a calibration cannot take place without any previous predictions available. This is the main reason for which the use of robust and generic turbulent schemes is the only way to reveal the weak points of turbulence modeling and suggest techniques for further improvement.

Based on the above remarks, the use of the standard k–ε turbulence model, in conjunction with nonequilibrium logarithmic wall functions, has been selected instead of a low-Reynolds scheme because it represents a good compromise between accuracy and computational time consumption, given that it requires no extra mesh refinement near the wall and produces quite accurate results, for engineering purposes. On the other hand, RSM improves prediction accuracy and provides analytical solutions for the Reynolds stress components directly comparable to experimental measurements, although it also significantly increases the computational cost (Brison and Brun, 1991; Launder and Spalding, 1974).

The numerical results reported here include predictions of the velocities and their fluctuations in the free-jet region, local Nusselt numbers in the circumferential direction, and velocity variations along the concave surface. The predictions are compared to the experiments of Choi et al. (2000), which can serve as a benchmarking data set for turbulence modeling on curved surfaces. Results show that both models can be applied to turbine blade design applications, with relative ease, yielding accurate predictions.

The Physical and Mathematical Model

Geometry

Figure 1 shows the computational domain used to model the experimental setup of Choi et al. (2000).

A 2-D slot nozzle with a 5-mm width (B) is used to produce an air jet, which impinges onto a semicircular concave surface with a diameter of 150 mm, on which a boundary condition of constant heat flux is applied. Figure 2 shows typical velocity contours on a plane parallel to the jet flow.

Mathematical Model

The k–ε Model. The k– ε model uses an eddy–viscosity hypothesis (Launder and Spalding, 1974) for the turbulence and relates the turbulence viscosity ν_T to the turbulence kinetic energy k and the turbulence dissipation rate ε, using

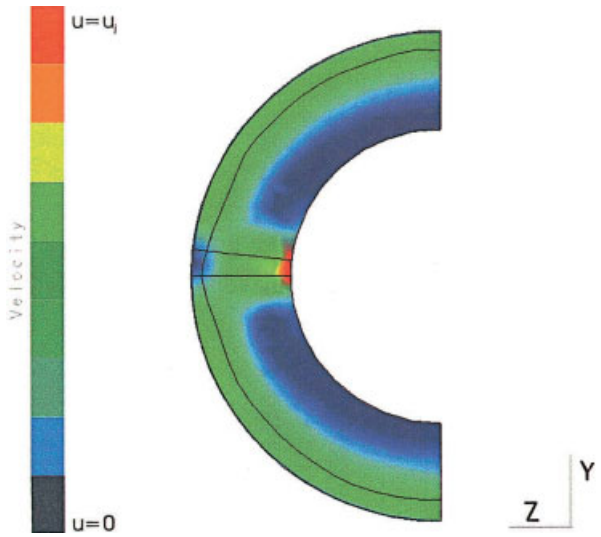

Figure 2. Typical velocity contours on a plane parallel to the jet flow.

$$\nu_T = C_\mu \frac{k^2}{\varepsilon} \tag{1}$$

The equations for k and ε are presented below

$$\frac{\partial(\rho U_i k)}{\partial x_i} = \frac{\partial}{\partial x_i}\left[\left(\mu + \frac{\mu_T}{\sigma_k}\right)\frac{\partial k}{\partial x_i}\right] - \rho\overline{u_i u_j}\frac{\partial U_i}{\partial x_j} - \rho\varepsilon \tag{2}$$

and

$$\frac{\partial(\rho U_i \varepsilon)}{\partial x_i} = \frac{\partial}{\partial x_i}\left[\left(\mu + \frac{\mu_T}{\sigma_k}\right)\frac{\partial \varepsilon}{\partial x_i}\right] - \overline{u_i u_j}\frac{\partial U_i}{\partial x_j}C_1\rho\frac{\varepsilon}{k} - C_2\rho\frac{\varepsilon^2}{k} \tag{3}$$

where U_i is the mean velocity in the i direction; u_i and u_j are the fluctuating velocities in the i and j direction, respectively; k is the turbulent kinetic energy; ε is the dissipation rate of turbulent kinetic energy; μ is the molecular dynamic viscosity; ν_T is the turbulent kinematic viscosity; and ρ is the density of the fluid. $C_\mu = 0.09$, $C_1 = 1.44$, and $C_2 = 1.92$ are k–ε turbulence model constants.

The Reynolds Stress Model (RSM). The Reynolds stress transport model (Launder et al., 1975) consists of a closed set of transport equations for the Reynolds stress $\overline{u_i u_j}$. The model equations may be written as

$$U_k\frac{\partial(\overline{u_i u_j})}{\partial x_i} = D_{ij} + G_{ij} + \Phi_{ij} - E_{ij} \tag{4}$$

where D_{ij}, G_{ij}, Φ_{ij}, and E_{ij} are, respectively, the diffusion, the stress production, the pressure–strain correlation, and the dissipation term. Hanjalic and Launder (1972) modeled the diffusion term as

$$D_{ij} = \frac{\partial}{\partial x_k}\left[C_{S1}\frac{k}{\varepsilon}\left(\overline{u_i u_j}\frac{\partial\overline{u_j u_k}}{\partial x_i} + \overline{u_j u_i}\frac{\partial\overline{u_i u_k}}{\partial x_i} + \overline{u_k u_i}\frac{\partial\overline{u_i u_j}}{\partial x_i}\right)\right] \tag{5}$$

where $C_{S1} = 0.22$.

The stress production term G_{ij} is defined by

$$G_{ij} = -\left(\overline{u_i u_k}\frac{\partial U_j}{\partial x_k} + \overline{u_j u_k}\frac{\partial U_i}{\partial x_k}\right) \tag{6}$$

The return-to-isotropy term $\Phi_{ij,1}$ and the rapid pressure–strain term $\Phi_{ij,2}$, given below, constitute the pressure–strain model of Launder et al. (1975)

$$\Phi_{ij} = \Phi_{ij,1} + \Phi_{ij,2} = -C_{S2}\frac{\varepsilon}{k}\left(\overline{u_i u_j} - \frac{2}{3}\delta_{ij}k\right) - C_{S3}\left(G_{ij} - \frac{1}{3}\delta_{ij}G_{kk}\right) \tag{7}$$

The first term, $\Phi_{ij,1}$, represents the contribution arising from the interaction between fluctuating quantities, whereas the second term, $\Phi_{ij,2}$, represents the contribution arising from the interaction between mean strain and fluctuating quantities. C_{S2} and C_{S3} are constants of the model, equal to 3.0 and 0.3, respectively.

E_{ij} represents the viscous destruction of $\overline{u_i u_j}$ and is modeled assuming local isotropy

$$E_{ij} = \tfrac{2}{3}\varepsilon\delta_{ij} \tag{8}$$

It should also be noted that "wall-reflection terms" are not used to calculate the influence of wall-reflected pressure fluctuations on the redistribution of the stresses. These terms are very complex and their effects are obscured within the solution of the RSM (Clarke and Wilkes, 1989; Wilkes and Clarke, 1987). Therefore, they have been omitted because they would affect the rate of convergence and increase turnover times.

Computational procedure

Calculations with three nozzle-to-target plane distances of H/B values of 4, 6, and 10 were performed to evaluate the effect of the spacing between the nozzle and the concave surface. In the first test case ($H/B = 4$), the target surface is inside the potential core, whereas in the second case ($H/B = 6$) and third case ($H/B = 10$) the target is near and outside the end of the potential core, respectively. The potential core is defined as the length of the region where the local velocity is maintained at not less than 95% of the jet velocity at the nozzle exit. In every one of the above cases the variation of the jet Reynolds number has been taken into consideration, making calculations for three different jet Reynolds numbers ($\mathrm{Re}_{2B} = 1780$, $\mathrm{Re}_{2B} = 2960$, and $\mathrm{Re}_{2B} = 4740$). The specific nozzle-to-surface distances and Reynolds numbers have been selected to match the experimental data of Choi et al. (2000).

The Nusselt number is calculated on the basis of the enthalpy equation as

$$\mathrm{Nu}_{2B} = \frac{h2B}{k_s} = \frac{q_w}{T_w - T_j}\frac{2B}{k_s} \tag{9}$$

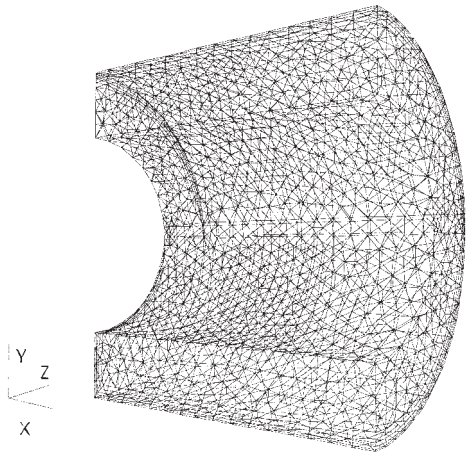

Figure 3. Unstructured computational grid.

Numerical details

The slot nozzle was modeled as a constant momentum inlet boundary condition and the Cartesian components of velocity on the inlet boundary were set according to the experiments of Choi et al. (2000). The simulated air jet impinges onto a semicircular concave surface with a diameter of 150 mm, which is modeled as a wall-type boundary condition of constant heat flux according to the experiments as well (Figure 1). All other surfaces are free and are treated as zero-pressure boundaries to allow the fluid to cross the boundary surface in either direction and model the end effects of the domain.

The runs were performed on a Silicon Graphics network machine with eight R10000 processors at the National Technical University of Athens, using an F77 FORTRAN compiler. The numerical procedure was based on a finite-volume solution of the elliptic mean momentum, energy, and turbulent transport equations, using the SIMPLE algorithm (Patankar, 1980; Patankar and Spalding, 1972) on a nonstaggered fully unstructured grid. The convection terms in the momentum equations were approximated using a QUICK differencing scheme.

The Grid

A fully unstructured grid was used for the simulations (Figure 3). This type of grid is a hybrid one that contains 3D element shapes of various types (prisms, pyramids, tetrahedrons). In viscous flows, the resolution of the thin diffusion layers close to the domain boundaries imposes extra requirements to the grid generator that can be met only by hybrid meshes (for example, Garimella and Shephard, 2000). Hybrid grid approaches came from the unstructured grid community in cases where it is recognized that the structured-like grid (prismatic grid) should be embedded underneath an otherwise unstructured grid, to better resolve the viscous region (Holmes and Connell, 1989).

More analytically, the mix of different cells is used to produce a more computationally efficient mesh near the wall boundaries of the domain, where velocity gradients are large normal to the surface, but small parallel to it. If only tetrahedral elements were used, a prohibitively fine surface mesh would be required to avoid generating highly distorted tetrahedral elements at the surface. The grid generator used in the present study overcomes this problem by using prismatic elements to create a mesh that is finely resolved normal to the wall, but coarse parallel to it. 2-D triangular surface elements are extruded into three-dimensional prisms at selected walls, thus producing a beneficial and cost-effective mesh arrangement.

In the present study, before proceeding with the experimental data comparison, additional grid sensitivity tests were carried out. For each one of the three geometries studied, the performance of six different meshes was tested. Results indicated for all geometries that the calculated Nusselt number values between the selected and a finer grid, in each case, were practically identical. In all grids tested selection of the turbulence model did not appear to particularly influence the grid independence of the results. For example, for the geometry of $H/B = 4$, 5180 grid elements were preferred and used instead of 5948 grid elements that substantially increased the computational requirements (33% increase in total CPU time, using standard k– ε) without practical differences in the Nusselt number predictions.

These tests showed that the numerical predictions are grid independent for the following resolutions:

- Geometry of $H/B = 4$: total number of 5180 grid elements, consisting of 2150 tetrahedrons, 43 pyramids, and 2987 prisms.
- Geometry of $H/B = 6$: total number of 7756 grid elements, consisting of 3434 tetrahedrons, 70 pyramids, and 4252 prisms.
- Geometry of $H/B = 10$: total number of 12,793 grid elements, consisting of 5631 tetrahedrons, 112 pyramids, and 7050 prisms.

The main reason for using an unstructured grid method is related to the complexity of the simulated geometry, as well as to the simplicity and ease of implementation that these methods present compared to structure mesh generation methods. The suggested way of meshing has been proved to be an effective tool to optimize an industrial process of concave jet impingement, without laying out block structure or connections.

Computational cost

By comparing the computational power needed for each turbulence models under consideration (k– ε and RSM), it was found that the implementation of the Reynolds stress model demanded an extra cost of 22% CPU time, compared to that of the standard k– ε model.

Results and Discussion

Free-jet and wall-jet profiles are presented for three different nozzle-to-target plane heights ($H/B = 4$, $H/B = 6$, and $H/B = 10$), and three Reynolds numbers tested (Re_{2B} values of 1780, 2960, and 4740). The inlet conditions for the computations were based on the experimental data of Choi et al. (2000), using a top-hat profile for inlet axial velocities.

Turbulence characteristics

Free Jet. Figure 4 shows a comparison between experimental (Choi et al., 2000) and computational results for the axial mean velocity along the centerline for the three H/B ratios and three Reynolds numbers. The values in the figures have been nondimensionalized using the jet velocity at the center of

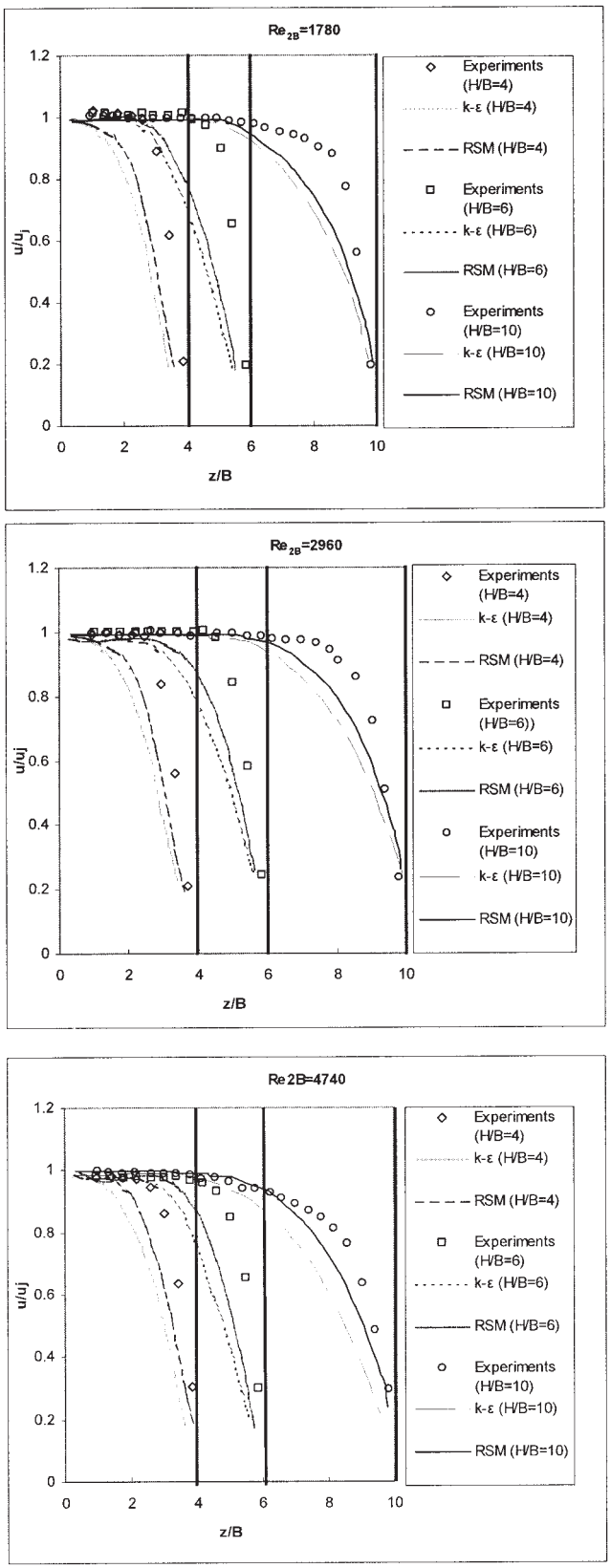

Figure 4. Axial mean velocity predictions along the centerline.

the nozzle exit (U_j) and the two-dimensional slot jet width (B = 5 mm). The lines printed in bold in Figure 4 designate the location of the concave wall for each H/B tested.

The predicted free-jet results are qualitatively in good agreement with the experimental data, especially the predictions obtained by the Reynolds stress model. Both models seem to capture quite accurately the standard top-hat profile close to the nozzle exit. However, both models considerably overestimate the rate of velocity decay, with the RSM predicting a slower decay than that of the standard k–ε. Both models predict an earlier start of the decay of the mean axial velocity along the centerline. This in turn, leads to an underprediction of the potential core length. The predicted results deviate from the experiments at least one order of magnitude, with this disagreement being higher for the geometries of H/B values of 4 and 6. As the Reynolds number is increased, the RSM shows its advantages over the k–ε model, yielding values of the axial mean velocity closer to experimental values. The underprediction of the potential core length results in the prediction of a larger stagnation region thickness, which is the thickness of the region where a velocity profile deviates from the free-jet characteristics. Choi et al. (2000) measured a stagnation region thickness of approximately $2B$, whereas the predictions yield a thickness of $3.5B$ for the k–ε model and around $3B$ for the Reynolds stress model.

Both models overpredict the spreading rate of the jet because of an overprediction of the entrainment of ambient air into the jet, with the RSM model being closer to the experimental results. This is consistent with previous flat-plate impingement studies (Malin, 1988; Rodi, 1980), which reported that all k–ε models overpredict the free-jet spreading by some 25% because of deficiencies in the ε-transport equation.

The axial velocity fluctuations along the centerline, calculated with the RSM, are compared to the experimental values in Figure 5. The RSM reproduces the shapes of the experimental curves, but underpredicts the experimental values approaching to the concave wall. The RSM also fails to calculate correctly the rate of decay of axial velocity fluctuations. This is attributed to the use of the standard wall function in the RSM. A wall submodel, such as the one used in the low-Reynolds k–ε turbulence models, would result in local improvement of predicted results.

However, predicted values are higher than the experimental ones, in the potential core region, indicating the inability of the model to capture the details of turbulence dispersion. The increased ambient air entrainment predicted in this region results in underprediction of the spreading rate of the jet (in agreement with Figure 4). The trend (that is, overprediction of axial velocity fluctuations close to the jet-issuing region and underprediction of the values as the target concave surface is approached) is not dependent on the Reynolds number (see Figure 5).

For comparison purposes the velocity fluctuations, calculated with both turbulence models, are presented in Figure 6 for all three different spacings tested at Re_{2B} = 2960. The k–ε values were calculated from the values of the turbulent kinetic energy (k), assuming local isotropy. It is quite evident that despite the failure of both models to accurately estimate the peak of the velocity fluctuation, the RSM predictions yield significantly more accurate results, especially away from the wall. Both turbulence models yield much better agreement with

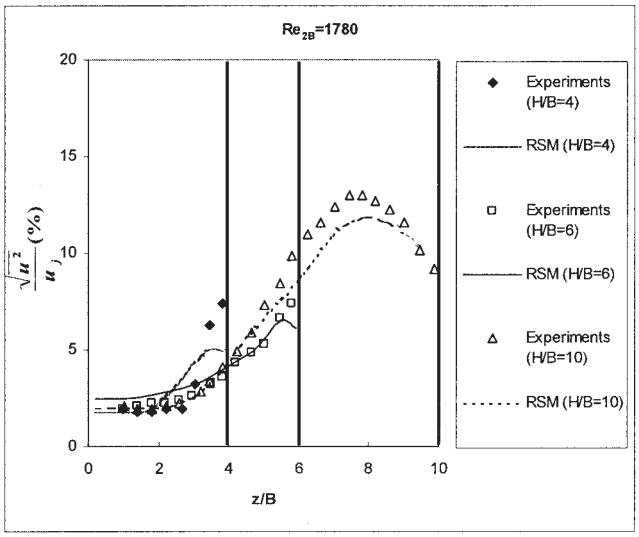

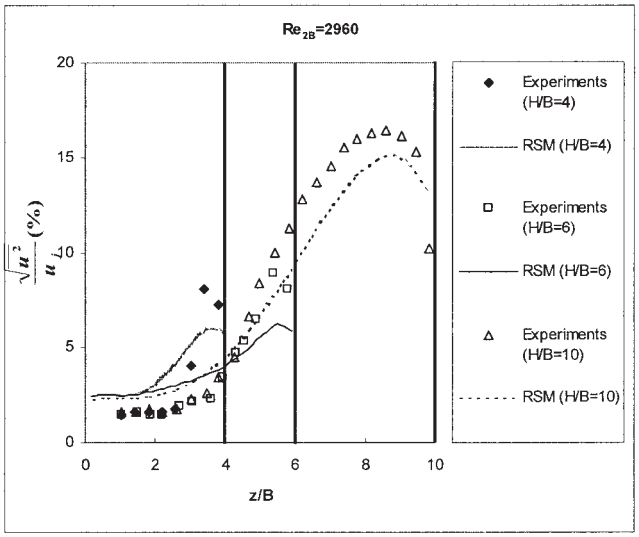

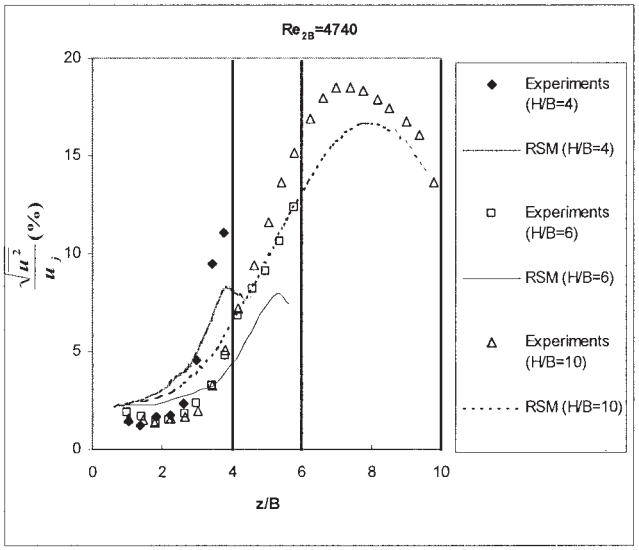

Figure 5. RSM predictions of normalized velocity fluctuations along the centerline.

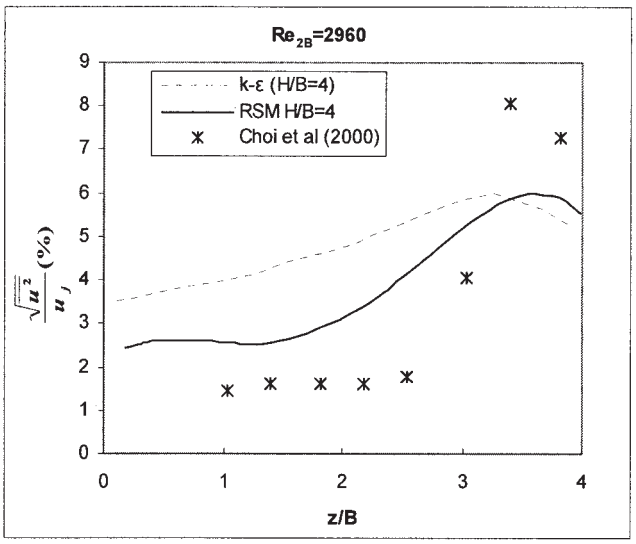

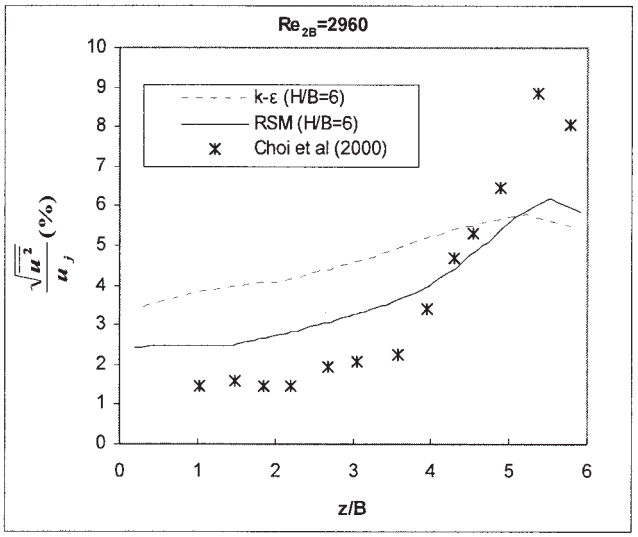

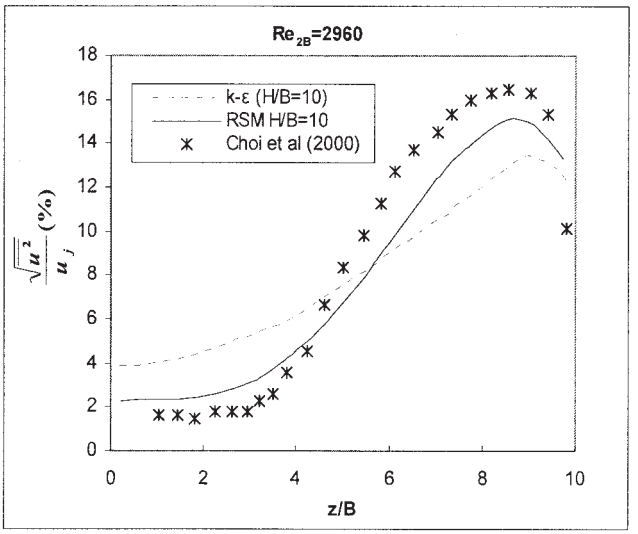

Figure 6. RSM and k–ε predictions of normalized velocity fluctuations along the centerline.

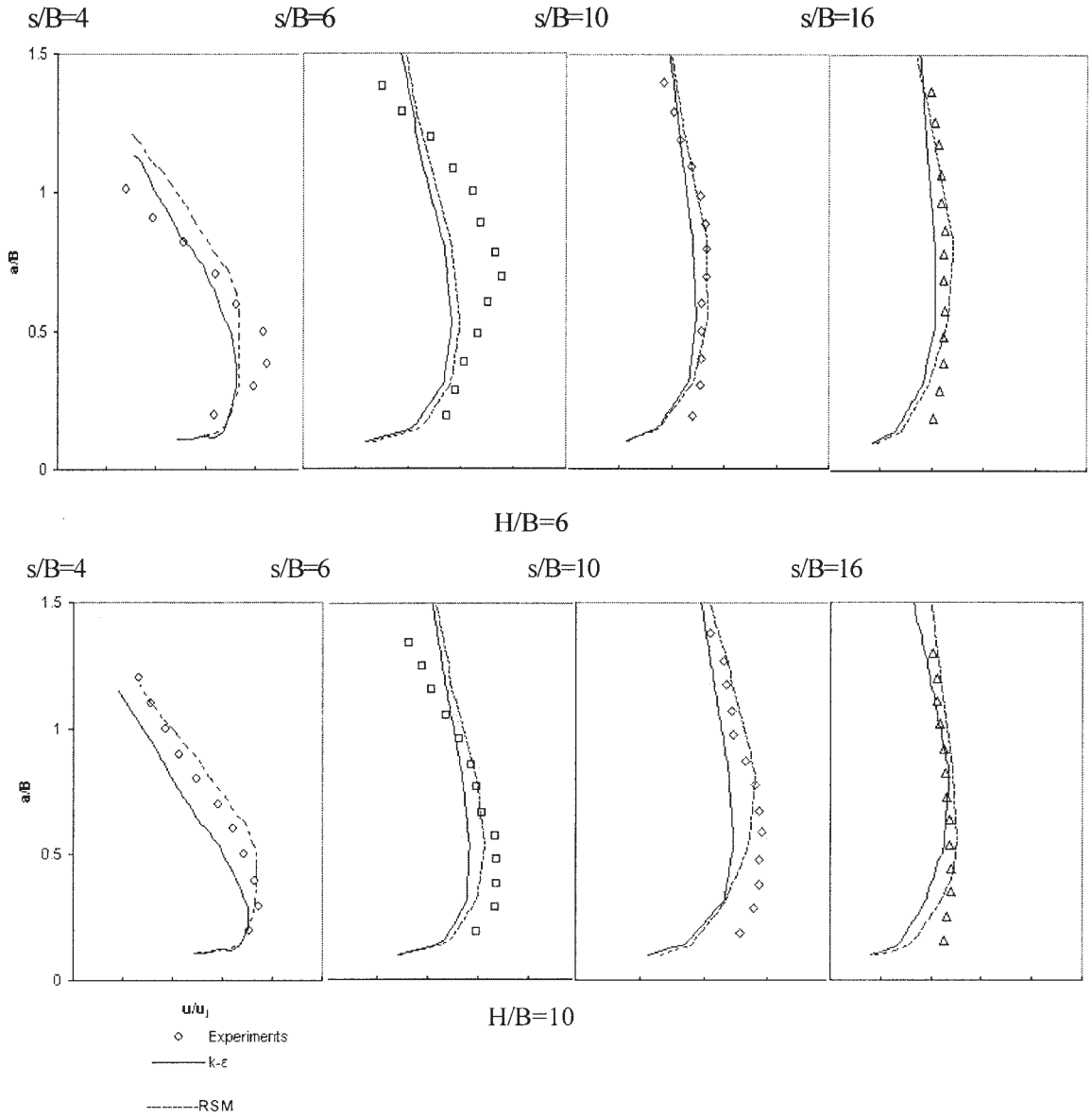

Figure 7. Mean velocity variations of wall-jet flow along the concave surface at Re_{2B} = 2960.

experiments when the nozzle-to-concave target spacing is increased.

Wall Jet. Figure 7 shows the axial mean velocity in the circumferential direction, in the wall jet region at $Re_{2B} = 2960$, for two different spacings ($H/B = 6$ and $H/B = 10$). The values of s/B on the upper side of Figure 7 designate the origin of the result for each s/B. There is a definite improvement in predictions with both models, moving away from the stagnation point in the circumferential direction, with the best matching to the experiments occurring at $s/B = 16$. This is attributed to the accurate prediction of the wall boundary layer. In a comparison of the two turbulence models, the RSM seems to be producing results that better match the trends of the experiments. For $s/B = 4$ and perpendicular distances of $0.3 < a/B < 0.6$ (that is, close to the stagnation point), both k–ε and RSM have the same behavior in any of the two geometries simulated, failing to match the shape of the experimental curves, by predicting smaller values and a steeper velocity drop compared to those of the experiments. In a comparison of the two models, the RSM is closer to the experimental data than the standard k–ε. Moving farther away from the wall ($a/B > 0.6$) the RSM model overpredicts the mean velocity values (especially in the case of $H/B = 6$), but is definitely closer to the experiments than the standard k– ε model, which substantially underpredicts measurements in the geometry of $H/B = 6$, and shows a composite behavior at $s/B = 4$, underpredicting the experimental data for $0.6 < a/B < 0.8$ and overpredicting them for vertical distances greater than $0.8B$ from the wall.

At $s/B = 6$ the distance between the nozzle and the target wall appears to be influencing the accuracy of the predictions. More specifically, for $H/B = 6$ the problematic behavior of both models is located in the area of perpendicular distances between $0.48B$ and B, whereas for $H/B = 10$ this area is seriously narrowed down between $0.3B$ and $0.6B$. In a com-

parison of the two models, the RSM again appears to be closer to the experimental data.

Finally, near the wall, both models underpredict the mean velocity of the wall jet along the concave surface.

Computations confirmed that no fluid acceleration is taking place, a finding that is in agreement with the experimental measurements of Choi et al. (2000), who measured mean velocities larger than the nozzle exit velocity only for spacings smaller than one nozzle slot jet width.

Heat Transfer. Figure 8 shows stagnation Nusselt numbers as a function of Reynolds number and of the impinging distance normalized by the nozzle width (H/B). Based on the three spacings modeled, the following general conclusions can be drawn:

- For each Reynolds number tested, the highest Nusselt numbers appear to occur at the spacing of $H/B = 6$.
- The maximum heat transfer rate is occurring at the highest Reynolds number ($Re_{2B} = 4740$), a fact obviously connected with the augmentation of the turbulence level.

In all cases both turbulence models quite satisfactorily predict the trend of the experimental data, but substantially underpredict measurements, with the RSM predictions being generally closer to reality than those of k–ε. This underprediction can be attributed to the calculation of lower values of mean velocities (see Figure 7) compared to experimental values.

Figure 9 shows the distribution of local Nusselt numbers along the streamwise direction for the three spacings tested at $Re_{2B} = 4740$. To explain the variations of local heat transfer in this direction a closer look at Figure 7 is required, although the two sets of figures refer to different Reynolds numbers (Figure 7: $Re_{2B} = 2960$; Figure 9: $Re_{2B} = 4740$). Such a comparison is valid, given that computations revealed the same trends for both Reynolds numbers, and was taken because of a lack of experimental data for the circumferential velocity for a Reynolds number equal to 2960.

By comparing Figure 7 to Figure 9, it is evident that the underprediction of heat transfer values must be attributed to the computation of significantly smaller velocity values, by both turbulence models (see Figure 7). This underprediction becomes more severe for circumferential distances between 3 and 10 nozzle slot jet widths ($3 < s/B < 10$), and thus in the area in which both models' predictions of mean velocity values was characterized earlier, as rather problematic and substantially underpredictive. Moving farther away from this region ($s/B > 10$), the prediction of significantly more accurate mean velocity values leads to a similar improvement in the computational accuracy for the local Nusselt numbers, with the RSM being generally closer than the two-equation k–ε model to experimental values.

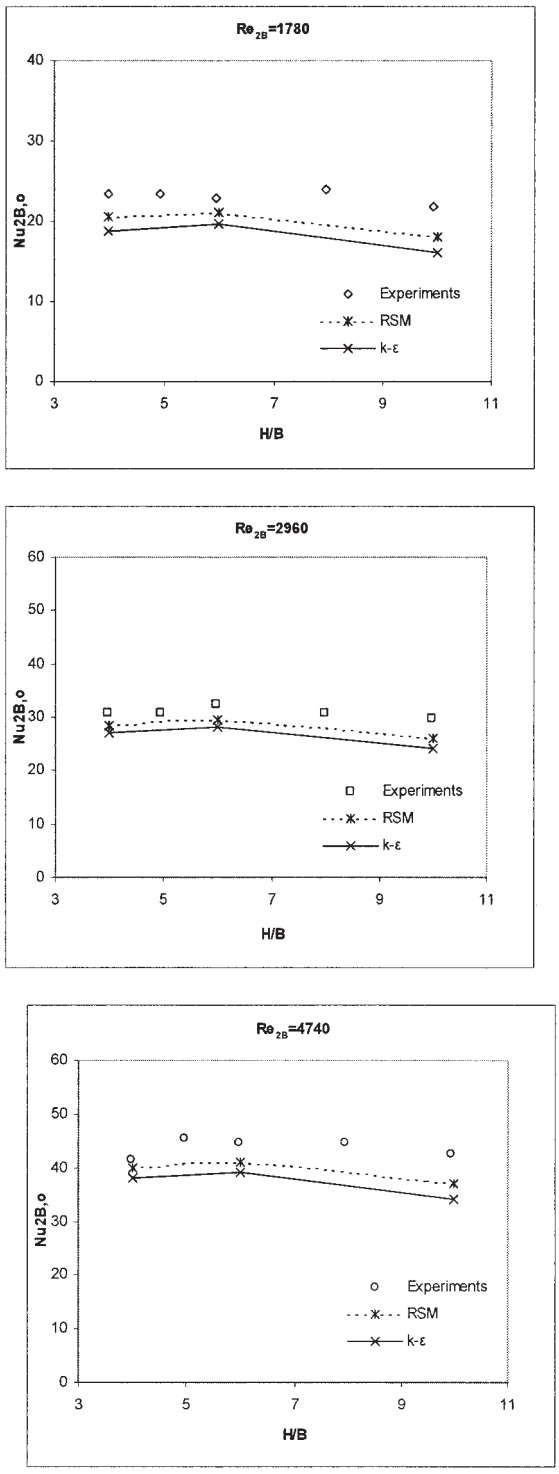

Figure 8. Variation of stagnation point Nusselt numbers for different H/B values.

Conclusions

Numerical predictions of the flow field generated by a turbulent jet impinging on a concave surface were obtained using a two-equation turbulence model and a Reynolds stress model. Results were validated by comparison with experimental measurements and confirm the following results:

- Satisfying agreement between numerical predictions and experiments can be achieved with the combination of an unstructured grid and any of the two turbulence models tested. The proposed model can serve as an excellent low-cost simulation tool to predict turbulent and heat transfer characteristics of concave jet impingement, without conducting time-consuming, difficult, and expensive experiments.
- The use of the RSM model did not dramatically improve the accuracy of predictions, apart from the case of fluctuating velocity calculations, where k–ε failed to estimate accurately

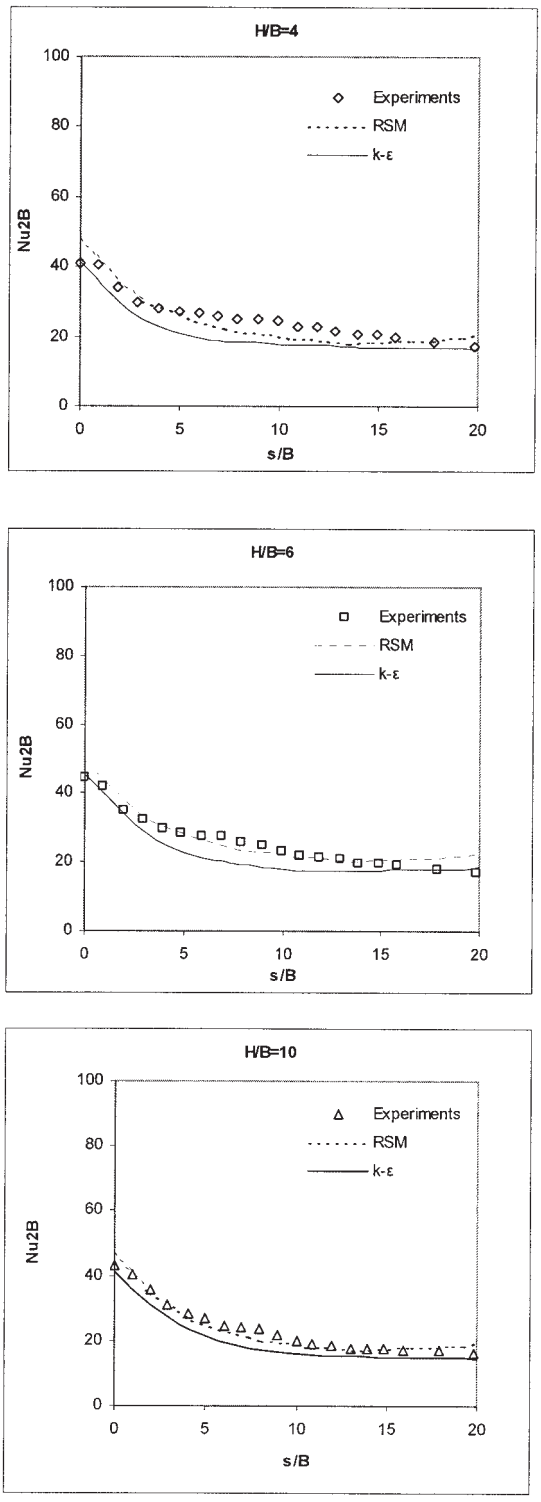

Figure 9. Distribution of local Nusselt numbers in the circumferential direction at Re_{2B} = 4740.

the experimental data. In all other cases both models performed similarly, both showing good agreement with the experimental data. Taking into account that (1) RSM is not as easy to incorporate into a CFD code as the k– ε model and (2) RSM is computationally more expensive (requires approximately 22% extra time), the modeler can take advantage of the simplicity and low computational requirements of the k–ε model, in cases where high accuracy is not the dominating factor.

- For both models, discrepancies between experiments and predictions increase, as the nozzle-to-target distance is decreased from 10 to 4 nozzle slot jet widths. The variation of the Reynolds number had no significant influence on the predictions.
- Accurate prediction of the wall boundary layer characteristics improves calculations with both models, away from the stagnation point and in the circumferential direction.
- The maximum heat transfer occurred at the highest Reynolds number, attributed to turbulence level augmentation. For the same Reynolds number maximum heat transfer occurs at $H/B = 6$. In all cases both models predict the trend of the experimental data quite accurately, but underpredict measurements because of the calculation of smaller mean and fluctuating velocity values in both the free-jet and wall-jet regions.

Notation

A = Coordinate perpendicular to the concave surface
B = Two-dimensional slot jet width (=5 mm)
C_{S1}, C_{S2}, C_{S3} = Reynolds stress model constants
C_μ, C_1, C_2 = k–ε turbulence model constants
D = Diffusion term
E = Dissipation term
G = Stress production term
h = Convection heat transfer coefficient
H = Distance from impingement concave surface
k_s = Thermal conductivity
k = Turbulent kinetic energy
Nu_{2B} = Nusselt number ($Nu_{2B} = h2B/k_s$)
$Nu_{2B,o}$ = Nusselt number at stagnation point
q_w = Heat flux on the heating surface
Re_{2B} = Jet Reynolds number at nozzle exit ($=U_{avg}2B/\nu$)
S = Circumferential distance from the stagnation point
T_j = Jet temperature
T_w = Wall temperature
U_{avg} = Area averaged jet velocity at the nozzle exit
u = Fluctuating velocity
U = Jet axial mean velocity
U_j = Jet velocity at the center of the nozzle exit
x, y, z = Coordinates
Z = Distance from the nozzle exit

Greek letters

δ_{ij} = Kronecker delta (=1 for $i = j$ and 0 for $i \neq j$)
ε = Dissipation rate of turbulent kinetic energy
μ = Molecular dynamic viscosity
μ_T = Turbulent dynamic viscosity
ν = Kinematic viscosity
ν_T = Turbulent kinematic viscosity
ρ = Density
σ_k = k–ε turbulence model constant
Φ = Pressure–strain scalar-variable term
Φ_{ij} = Pressure–strain correlation term

Subscripts

i, j, k = Indices for coordinate notation

Literature Cited

Barata, J. M. M., D. F. G. Durao, and J. J. McGuirk, "Numerical Study of Single Impinging Jets through a Crossflow," *J. Aircraft*, **26**(11), 1002 (1989).

Bray, D., "Jets in Cross-Flow and Ground Effect," Ph.D. Thesis, Aerome-

chanical Systems Group, Cranfield Institute of Technology, Shrivenham, Wiltshire, U.K. (1992).
Brison, J. F., and G. Brun, "Round Normally Impinging Turbulent Jets," Proc. of 15th Meeting IAHR Working Group on Refined Flow Modeling, Laboratoire Mécanique Fluides, ECL, Lyon, France (1991).
Bunker, R. S., and D. E. Metzger, "Local Heat Transfer in Internally Cooled Turbine Airfoil Leading Edge Regions. Part I: Impingement Cooling without Film Coolant Extraction," *ASME J. Turbomachinery*, **12**, 451 (1990).
Chien, K. T., "Predictions of Channel and Boundary Layer Flows with a Low Reynolds Number Turbulence Model," *AIAA J.*, **20**(1), 33 (1982).
Childs, R. E., and D. Nixon, "Turbulence and Fluid/Acoustic Interaction in Impinging Jets," SAE paper no. 872345 (1987).
Choi, M., H. S. Yoo, G. Yang, J. S. Lee, and D. K. Sohn, "Measurements of Impinging Jet Flow and Heat Transfer on a Semi-Circular Concave Surface," *Int. J. Heat & Mass Transfer*, **43**(10), 1811 (2000).
Chup, R. E., H. E. Helms, P. W. Mcfadden, and T. R. Brown, "Evaluation of Internal Heat Transfer Coefficients for Impingement-Cooled Turbine Airfoils," *J. Aircraft*, **6**, 203 (1969).
Clarke, D. S., and Wilkes, N. S., "The Calculation of Turbulent Flows in Complex Geometries Using a Differential Stress Model," Atomic Energy Research Establishment Report 13428, Berkshire, U.K. (1989).
Cornaro, C., A. S. Fleischer, and R. J. Goldstein, "Flow Visualization of a Round Jet Impinging on Cylindrical Surfaces," *Exp. Therm. Fluid Sci.*, **20**(2), 66 (1999).
Craft, T. J., L. J. Graham, and B. E. Launder, "Impinging Jet Studies for Turbulence Model Assessment—II. An Examination of the Performance of Four Turbulence Models," *Int. J. Heat & Mass Transfer*, **36**(10), 2685 (1993).
Dotoya, D., and P. Michard, "A Problem for Calculating Boundary Layers along Compressor and Turbine Blades," *Numerical Methods of Heat Transfer*, Wiley, New York (1981).
Dyban, Y., and P. Mazur, "Heat Transfer from a Flat Air Jet Flowing into a Concave Surface," *Heat Transfer—Soviet Res.*, **2**, 15 (1970).
Garimella, R. V., and M. S. Shephard, "Boundary Layer Mesh Generation for Viscous Flow Simulations," *Int. J. Numerical Methods Eng.*, **49**, 193 (2000).
Garimella, S., and B. Nenaydykh, "Nozzle-Geometry Effects in Liquid Jet Impingement Heat Transfer," *Int. J. Heat & Mass Transfer*, **39**(14), 2915 (1996).
Gau, C., and C. M. Chung, "Surface Curvature Effect on Slot Air-Jet Impingement Cooling Flow and Heat Transfer Process," *ASME J. Heat Transfer*, **113**, 858 (1991).
Hanjalic, K., and B. E. Launder, "A Reynolds Stress Model of Turbulence and Its Application to Thin Shear Flows," *J. Fluid Mechanics*, **52**, 609 (1972).
Hassid, S., and M. Poreh, "A Turbulent Energy Model for Flows with Drag Reduction," *Trans. ASME J. Fluid Eng.*, **100**, 107 (1978).
Hoffman, G. H., "Improved Form of the Low Reynolds Number k–ε Turbulence Model," *Physics of Fluids*, **188**, 309 (1975).
Holmes, D. G., and S. D. Connell, "Solution of the 2D Navier–Stokes Equations on Unstructured Adaptive Grids," Proc. of AIAA 9th CFD Conference, AIAA paper 89-1932, Buffalo, NY (1989).
Hrycak, P., "Heat Transfer from a Row of Jets Impinging on Concave Semi-Cylindrical Surfaces," *Int. J. Heat & Mass Transfer*, **28**, 175 (1981).
Hrycak, P., "Heat Transfer and Flow Characteristics of Jet Impinging on a Concave Hemispherical Plate," Proc. of the International Heat Transfer Conference, pp. 357–362 (1982).
Hsueh, K. L., and D. T. Chin, "Mass Transfer on a Submerged Jet Impinging on a Cylindrical Surface," *J. Electrochem. Soc.*, **133**, 1845 (1986).
Hwang, C. J., and J. L. Liu, "Numerical Studies of Two-Dimensional Impinging Jet Flow-Fields," *AIAA J.*, **27**(7), 841 (1989).
Jambunathan, K., E. Lai, M. A. Moss, and B. L. Button, "A Review of Heat Transfer Data for Single Circular Jet Impingement," *Int. J. Heat & Fluid Flow*, **13**, 106 (1992).
Knowles, K., "Computational Studies of Impinging Jets Using k–ε Turbulence Models," *Int. J. Numerical Methods in Fluids*, **22**(8), 799 (1996).
Kornblum, Y., and R. J. Goldstein, "Jet Impingement on Semi-Cylindrical Concave and Convex Surfaces. Part Two: Heat Transfer," Proc. Int. Symp. on Physics of Heat Transfer in Boiling and Condensation, pp. 597–602 (1997).
Koronaki, E. D., H. H. Liakos, M. A. Founti, and N. C. Markatos, "Numerical Study of Turbulent Diesel Flow in a Pipe with Sudden Expansion," *Appl. Math. Modell.*, **25**(4), 319 (2001).
Kottke, V., "Taylor–Görtler Vortices and Their Effect on Heat and Mass Transfer," Proc. Eighth International Heat Transfer Conference, **3**, pp. 1139–1144 (1997).
Lam, C. K. G., and K. A. Bremhorst, "Modified Form of the k–ε Model for Predicting Wall Turbulence," *Trans. ASME J. Fluids Eng.*, **103**, 456 (1981).
Launder, B. E., G. J. Reece, and W. Rodi, "Progress in the Development of a Reynolds Stress Turbulence Closure," *J. Fluid Mech.*, **68**, 537 (1975).
Launder, B. E., and B. I. Sharma, "Application of the Energy Dissipation Model of Turbulence to the Calculation of Flow Near a Spinning Disk," *Lett. Heat & Mass Transfer*, **1**, 131 (1974).
Launder, B. E., and D. B. Spalding, "The Numerical Computations of Turbulent Flows," *Comput. Methods Appl. Mech. Eng.*, **3**, 269 (1974).
Lee, D. H., Y. S. Chung, and D. S. Kim, "Turbulent Flow and Heat Transfer Measurements on a Curved Surface with a Fully Developed Round Impinging Jet," *Int. J. Heat & Fluid Flow*, **18**(1), 160 (1997).
Lee, D. H., Y. S. Chung, and S. Y. Won, "Technical Note: The Effect of Concave Surface Curvature on Heat Transfer from a Fully Developed Round Impinging Jet," *Int. J. Heat & Mass Transfer*, **42**(13), 2489 (1999).
Liakos, H. H., M. A. Founti, and N. C. Markatos, "Modeling of Stretched Natural Gas Diffusion Flames," *Appl. Math. Modell.*, **24**(5–6), 419, 2000.
Liakos, H. H., M. K. Koukou, M. A. Founti, and N. C. Markatos, "Effects of Pressure and Impingement Angle in Flaming Processes," *Can. J. Chem. Eng.*, **78**, 834 (2000).
Liu, T., and J. P. Sullivan, "Heat Transfer and Flow Structures in an Excited Circular Impinging Jet," *Int. J. Heat & Mass Transfer*, **39**(17), 3695 (1996).
Malin, M. R., "Prediction of Radially Spreading Turbulent Jets," *AIAA J.*, **26**(6), 750 (1988).
Martin, H., "Heat and Mass Transfer between Impinging Gas Jets and Solid Surface," *Adv. Heat Transfer*, **13**, 1 (1977).
Mayle, R. E., M. F. Blair, and F. C. Kopper, "Turbulent Boundary Layer Heat Transfer on Curved Surfaces," *ASME J. Heat Transfer*, **101**, 521 (1981).
Metzger, D. E., R. T. Baltzer, and C. W. Jenkins, "Impingement Cooling Performance in Gas Turbine Airfoils Including Effects of Leading Edge Sharpness," *ASME J. Eng. Power*, **94**, 219 (1972).
Metzger, D. E., T. Yamashita, and C. W. Jenkins, "Impingement Cooling on Concave Surfaces with Lines of Circular Air Jets," *ASME J. Eng. Power*, **91**, 149 (1969).
Myszko, M., "Experimental and Computational Studies of Factors Affecting Impinging Jet Flow Fields," PhD Thesis, Cranfield University, Shrivenham, U.K. (1997).
Patankar, S. V., *Numerical Heat Transfer and Fluid Flow*, Hemisphere, Washington, DC, pp. 126–134 (1980).
Patankar, S. V., and D. B. Spalding, "A Calculation Procedure for Heat, Mass and Momentum Transfer in Parabolic Flows," *Int. J. Heat & Mass Transfer*, **15**, 1787 (1972).
Reynolds, W. C., "Computation of Turbulent Flows," *Annu. Rev. Fluid Mech.*, **8**, 183 (1976).
Rodi, W., *Turbulence Models and Their Application in Hydraulics—A State of the Art Review*, International Association for Hydraulic Research, Delft, The Netherlands (1980).
Souris, N. E., H. H. Liakos, M. A. Founti, J. A. Palyvos, and N. C. Markatos, "Study of Impinging Turbulent Jet Flows Using the Isotropic Low-Reynolds Number and the Algebraic Stress Methods," *Comput. Mechanics*, **28**, 381 (2002).
Tabakoff, W., and W. Clevenger, "Gas Turbine Blade Heat Transfer Augmentation by Impingement of Air Jets Having Various Configurations," *ASME J. Eng. Power*, **94**, 51 (1972).
Thomann, H., "Effect of Streamwise Wall Curvature on Heat Transfer in a Turbulent Boundary Layer," *J. Fluid Mechanics*, **33**, 283 (1968).
Viskanta, R., "Heat Transfer to Impinging Isothermal Gas and Flame Jets," *Exp. Therm. Fluid Sci.*, **6**, 111 (1993).

Wilcox, D. C., and W. M. Rubesin, "Progress in Turbulence Modeling for Complex Flow-Fields Including Effects of Compressibility," *NASA Technical Paper* 1517 (1980).
Wilkes, N. S., and D. S. Clarke, "Turbulent Flow Predictions Using Algebraic Stress Model," Atomic Energy Research Establishment Report 12694, Berkshire, U.K. (1987).
Yang, G., M. Choi, and J. S. Lee, "An Experimental Study of Slot Jet Impingement Cooling on Concave Surface, Effects of Nozzle Configuration and Curvature," *Int. J. Heat & Mass Transfer*, **42**(12), 2199 (1999).

Manuscript received Sept. 10, 2002, and revision received Dec. 2, 2003.